Journal of
Mechanics of
Materials and Structures

MACROSCOPIC ELASTIC PROPERTIES OF RANDOMLY PACKED BALLOONS

Isao Taguchi and Michio Kurashige

Volume 2, Nº 3 March 2007

mathematical sciences publishers

JOURNAL OF MECHANICS OF MATERIALS AND STRUCTURES
Vol. 2, No. 3, 2007

MACROSCOPIC ELASTIC PROPERTIES OF RANDOMLY PACKED BALLOONS

ISAO TAGUCHI AND MICHIO KURASHIGE

Macroscopic elastic properties of sintered, randomly packed balloons are estimated for various degrees of sintering and for a wide range of balloon wall thickness. Macroscopic elastic moduli are little affected by a balloon's inner/outer diameter ratio for thicker balloons, while those of thinner balloons are very sensitive to the ratio. The elastic moduli rapidly decline with decreasing wall thickness. They are larger in the direction of gravity than in the horizontal one, corresponding to gravity-affected packing structures. Specific elastic moduli have a peak against porosity. Poisson's ratios are negative in some cases of very thin balloon walls and very low sintering degree. Comparison of the present random packing with the regular simple cubic packing reveals that there is a significant difference between them in their elastic properties and their structures of anisotropy, although both have almost the same coordination number.

1. Introduction

Cellular solids have many diverse applications such as hot gas and ion exchange filters, thermal protection systems, energy and sound absorption systems, heat exchangers, catalyst supports and porous implants for surgical treatments [Gibson and Ashby 1997; Ashby et al. 2000]. They may be regarded as porous materials with a very high porosity or very low solid volume fraction [Torquato 2001]. Among the cellular solids, foams are most commonly and widely used. The foams are usually classified by their pore type of either open or closed cells.

The open-cell foams are neither as stiff nor as strong as the closed-cell foams, and they allow fluids to flow through whereas the closed-cell foams do not. Because of this, they can be exploited in multifunctional applications of load supporting and heat dissipation [Wadley 2002; Queheillalt et al. 2002].

Open-cell metallic foams typically achieve mechanical behaviors close to theoretical predictions. Although the mechanical properties of closed-cell metallic foams theoretically exceed those of open-cell foams, defects reduce their measured properties to values similar to those for the open-cell foams [Andrews et al. 1999; Sanders and Gibson 2003b]. Bonded compacts of balloons may be a good alternative in terms of mechanical properties as well as in their ability to allow fluids to flow through connected pores.

In recent years, bonded compacts of balloons (or hollow spheres) made of ceramic, metal, inorganic glass, carbon, etc. have started to become commercially available and have been applied to various engineering practices [Torobin 1986; Norris and Gojny 1990; Andersen et al. 2000]. Because the materials made by bonding balloons contain both types of connected and closed pores, these structures have significant potential for those multifunctional applications which require a combination of impact energy absorption, acoustic attenuation [Gasser et al. 2004a] and/or thermal insulation, in addition to

Keywords: balloon, elastic modulus, random packing, transverse isotropy, negative Poisson's ratio, optimum design.

structural load support; the bonded balloons also have potential for improved mechanical properties and high-porosity structures, that is, for high specific stiffness and strength.

Another important usage of the microballoons is as syntactic foams, which are mixtures of microballoons and polymeric (or metallic) matrix material [Bardella and Genna 2001; Marur 2005]. Because the microballoons are dispersed in the matrix material, the syntactic foams are closed-cell foams and do not allow fluids to flow through connected pores. We will exclude the syntactic forms from the present argument.

Using the finite element method, Sanders and Gibson [2003b] analyzed the mechanical properties of simple cubic (SC) packed hollow-sphere foams, and compared them with those for the open-cell and closed-cell foams. The results indicated that the theoretical values of moduli and strength stand between those of the open- and closed-cell foams. Furthermore, they also obtained those of body-centered cubic (BCC) and face-centered cubic (FCC) packings [Sanders and Gibson 2003a]. It was found that the FCC packing gives the highest values of moduli and strength.

Like Sanders and Gibson [2003a], Gasser et al. [2003] investigated the uniaxial tensile elastic properties of regular FCC hollow sphere packings, and expressed three independent elastic constants of the materials for FCC stacking in terms of polynomial expressions [Gasser et al. 2004b]. They compared the results with the estimations from the formulae proposed by Sanders and Gibson [2003a]; it was shown that the polynomial expressions are valid for the case where the size of necks is much smaller than 0.2 times the balloon radius.

All of the above studies have dealt with regular stackings. However, bonded balloon aggregates are usually fabricated by dumping balloons into a container and in some cases by tapping it to obtain denser packings, leading to random structures. Thus, we need to take into account the randomness of balloon structures. It should be noted that the randomness hinders us from using the finite element analysis of such unit cells as those in SC, BCC and FCC stackings; we have to resort to another method.

For randomly packed solid spherical particles, Kurashige et al. [1999a] proposed a three-step simulation method. This method constructs a random packing of spheres in a computer by sequential deposition of them, followed by replacing the packing, after *sintering* it, by a three-dimensional random network of springs of six degrees of freedom, and then by estimating effective elasticity coefficients by conventional structural analysis. The results by this simulation were in good agreement with experimental ones. Moreover, Kato et al. [2002] extracted a statistical characteristic of the random packing structure from data on the random packing; although this kind of statistic is important to understand some relations between the packing structures and their macroscopic characteristics, it cannot be obtained in other models, such as the self-consistent models. They also estimated the mechanical properties (effective elastic moduli and elastic wave speeds) by the same evaluation method as that in Kurashige et al. [1999a]. From this evaluation, it was found that the packing structure of spherical particle random packings and the elastic property of sintered compacts are of transverse anisotropy, due to gravity. Furthermore, Kurashige et al. [1999b] applied the method to the thermal conductivity estimation of sintered solid particles; they confirmed the usefulness of their method.

The present paper treats elastic properties of the bonded balloon random packing. We deal here with the *sintered* balloons, which imply that the bonding material is identical to that of the balloons, but the present method is applicable to blazed balloon random packings, or those bonded by other methods. We carry out a thorough simulation using the above method [Kurashige et al. 1999a; Kato et al. 2002] to

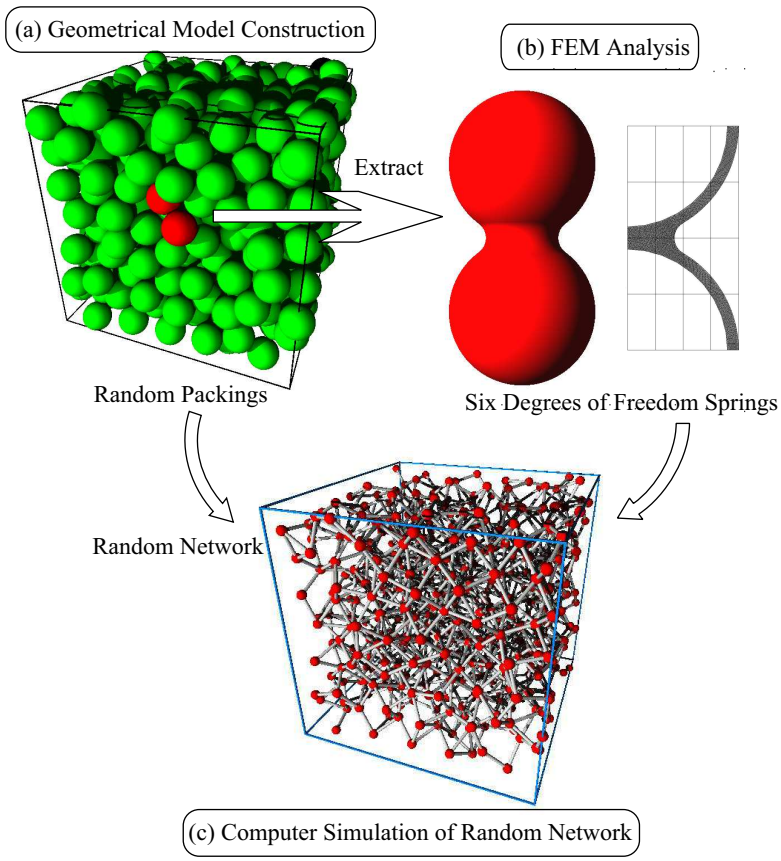

Figure 1. Three step simulation method: (a) geometrical model construction of randomly packed balloon aggregate by the method of a rigid sphere free fall into a virtual box; (b) evaluation of the characteristics of a microscopic structure by FEM analysis of spring constants for a sintered balloon pair; (c) simulation of macroscopic material properties by 3D structural analysis of a random network of springs, yielding desired macroscopic elastic moduli.

examine statistical characteristics of the balloon packings and their macroscopic elastic properties and to propose simple formulae to estimate the elasticities, by going through the following steps. (We will use the term *balloon packings*, although there is no difference in packing structures and their statistical characteristics between solid and hollow spheres.)

First, to generate a structural model of sintered balloon aggregates, we carry out a random packing simulation of the sequential accumulation method of equal-sized balloons into a virtual box (see Figure 1a) combined with the use of periodic boundary conditions and random ups and downs of the box floor

level. Some statistical characteristics of aggregate microstructures are examined by using such parameters as porosity, coordination number, cumulative frequency of diameters of the circles appearing on a cross-section created by cutting the aggregate and cumulative angular distribution of all contact points within the aggregate.

Next, we extract a pair of connected spheres from the packing and regard it as a spring with six degrees of freedom: one for elongation and torsion, and two for bending and shearing. Properties of the microstructure element (that is, spring constants) are estimated by the finite element method; see Figure 1b.

Finally, we carry out tensile and shear tests of a random network of springs, with rigid hinges, of six degrees of freedom with the spring constants already estimated by the finite element method (Figure 1c). From this simulation, we obtain the average tensile (or shear) stress and the average strain resulting from the applied load. Thus, the desired macroscopic Young's and shear moduli and Poisson's ratios are determined.

We also calculate Young's modulus for the SC packing using the present three-step method to confirm its validity. To consider an optimum design, macroscopic specific (that is, per weight) elastic moduli are precisely estimated for a wide range of balloon thickness and sintering degree. Furthermore, we compare the results for the present random packing with those for the regular packing obtained by Sanders and Gibson [2003b].

2. Geometrical model construction

2.1. ***Equation of motion.*** To generate a spherical particle random packing structure in a computer, we carry out the simulation by the method of rigid sphere free fall into a box. More details can be found in [Taguchi et al. 2006].

We sequentially release a spherical particle with diameter D from random positions into a virtual box in the computer. The motion equation of the sphere in a vectorial form can be expressed as:

$$c\frac{d\boldsymbol{x}}{dt} = k\Delta\boldsymbol{d} - mg\boldsymbol{k}, \tag{1}$$

where $\boldsymbol{x}$ is the position vector of a falling sphere's center, $\boldsymbol{k}$ is the unit vector along the z axis pointing upward and $\Delta\boldsymbol{d}$ is the overlapping depth vector of the sphere in collision with another still one. Constants c, k, m and g are the viscosity, the spring constant between two or more particles in collision, mass of each particle, and the gravitational acceleration, respectively. We solve equation Equation (1) by the Runge–Kutta–Gill method.

2.2. ***Simulation method.*** Consider the virtual box of $0 \le x \le B$, $0 \le y \le B$, $0 \le z \le H (B < H)$. We do not stop introducing balloons until the cubic region $0 \le x \le B$, $0 \le y \le B$, $0 \le z \le H$ is completely filled with balloons. For the box size $B/D = 16$ adopted, 5 runs were made with 5 different sets of pseudo-random numbers, giving 5 samples. Five lists of final coordinates of all balloons' centers will be used to analyze the statistical characteristics and to estimate the elastic moduli of sintered balloons later on.

The effects of the boundaries of the virtual box in which spheres accumulate are eliminated by introducing the cyclic boundary condition. The level of the box floor is moved up and down for each sphere

	$B/D = 16$
Sample 1	0.417439
Sample 2	0.417035
Sample 3	0.417106
Sample 4	0.416517
Sample 5	0.417406
Mean	0.417101
Standard deviation	0.000372

Table 1. Porosities of five samples; their mean and standard deviation.

by a magnitude given by pseudo-random numbers in order to avoid packing regularity on the floor. The algorithm by Wichmann and Hill [1982] is used for the generation of the random numbers.

3. Statistical characteristics of geometrical model

3.1. ***Porosity.*** Porosity associated only with interstitial void space between the hollow spheres is one of the most important parameters characterizing a random packing of particles. It should be cautioned that the porosity excludes hollow space in the hollow spheres. The porosity of the random packing constructed by the above method is evaluated from the center coordinate lists and shown in Table 1. As seen from this table, the mean porosity is about 41.7%. This mean value is in good agreement with that obtained by Kato et al. [2002].

In general, random packings are classified into three categories [Haughey and Beveridge 1969; Tory et al. 1973]: very loose random packing ($0.44 \le \phi \le 0.47$), random loose packing ($0.41 \le \phi \le 0.44$), and close random packing ($\phi \approx 0.36$).

The mean porosity shown in Table 1 reveals that our packings fall in the category of random loose packing. The porosity $\phi = 0.417$ obtained here is rather small in the range of the loose random packing, because the present method allows no bridging.

3.2. ***Coordination numbers.*** Next, we examine the coordination number for our random packings for the box size $B/D = 16$. The coordination number is defined as the number of contact points of a particle with neighboring ones in a regular or irregular packing of particles. With a few regular packings, it is 6 for the SC, 8 for BCC and 12 for FCC; in contrast, there is a possibility that a sphere is in contact with four to twelve other spheres for the random packing [Nolan and Kavanagh 1992].

Table 2 shows the mean coordination number for all particles for each sample and the mean value and standard deviation for the five samples. The mean value 6.019 is in good agreement with that obtained by Kato et al. [2002]. It is found that the average coordination number for the random packing constructed is very near to that for the regular SC packings.

Figure 2 shows the distribution of the coordination numbers for the five samples. From this figure, it can be seen that the coordination distribution has its peak at 6 and ranges from 4 — 8 for all samples;

	Coordination Number
Sample 1	6.016345
Sample 2	6.020791
Sample 3	6.020047
Sample 4	6.019235
Sample 5	6.020346
Mean	6.018755
Standard deviation	0.001921

Table 2. Coordination number for five samples; their mean and standard deviation.

it has negligibly small percentage for three and nine contact points and no sphere has more than then contact points. Little difference in the distribution can be seen among the samples.

3.3. ***Cumulative frequency of diameters of circles appearing on a cross-section.*** If a randomly packed aggregate of balloons is sectioned along a plane, a large number of double circles will appear on its resultant cross-section; the outer circles have various values of diameter D', which is naturally smaller than or equal to D. Cumulative distribution of the diameter $f(D'/D)$ is theoretically given by

$$f(D'/D) = 1 - \sqrt{1 - (D'/D)^2}, \tag{2}$$

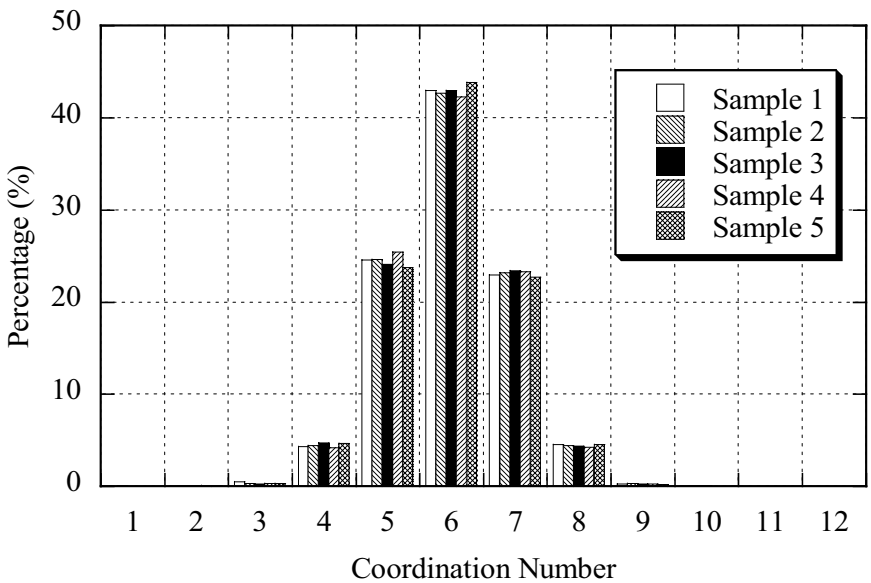

Figure 2. Coordination number distribution for all five samples.

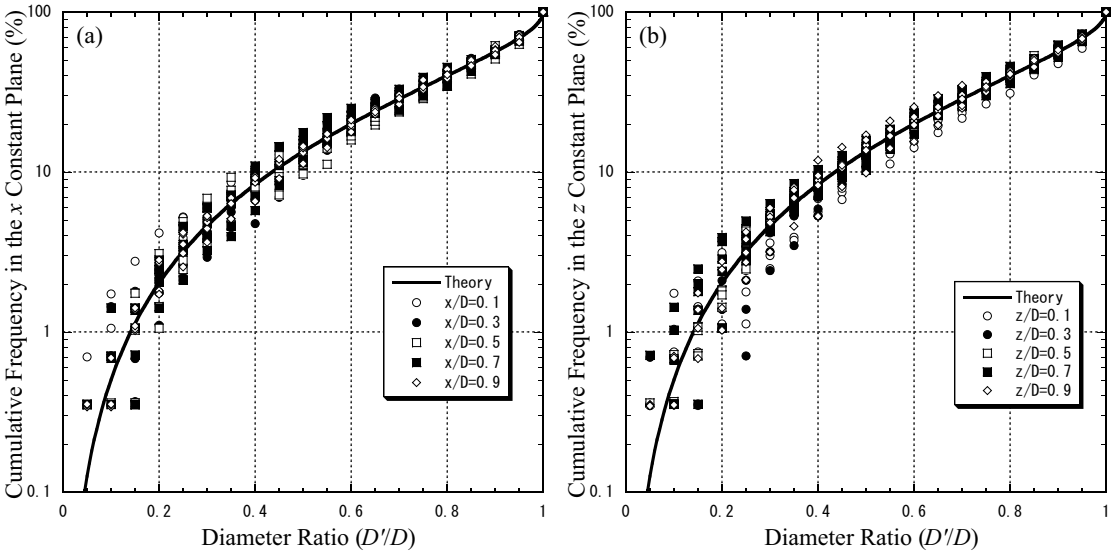

Figure 3. Cumulative frequencies of diameters of circles appearing on x and z cross sections created by cutting aggregate, corresponding to (a) and (b), respectively.

provided that the centers of packed balloons are distributed in a uniformly random manner [Debbas and Rumpf 1966; Bennett 1972].

Figures 3a and 3b show the cumulative frequencies of diameters of simulated random packings for all samples in terms of percentage for the x, z = constant cross sections, respectively. (The figure for y = constant is omitted because it is similar to that for x = constant). Here, the solid line is the theoretical prediction given by Equation (2). Each frequency is for each of five sectional planes x/D or $z/D = 0.1, 0.3, 0.5, 0.7$ and 0.9. It is seen that the frequencies scatter more around the theoretical value for the smaller diameter ratio. The scattering in [Kato et al. 2002] is smaller than the present one, because there the frequencies were calculated by averaging over the five sectional planes. The cumulative frequency for the z = constant planes is not different from that for the x = constant plane. This implies that the centers of spheres are almost uniformly randomly distributed equally along the three mutually orthogonal directions, although the scattering on the z = constant planes seems somewhat larger.

3.4. ***Distributions of branch orientations.*** A *branch* is defined as a segment connecting the centers of balloons in contact; the spheres are judged to be in contact if the length of branch is equal to or smaller than the diameter of sphere D, and not in contact if larger.

Although the sphere centers appear to be uniformly distributed as shown in the above subsection, it may be important to examine orientations of all branches.

Kato et al. [2002] examined distributions, not cumulative ones, of the branch orientations in the similar random packings. They divided the domain of zenithal and azimuthal angles into sub-domains by 10° step and calculated both the angular frequencies for each step, which were depicted in the form of a bar chart. They concluded that the peak in the zenithal distributions appears around 45° from the vertical

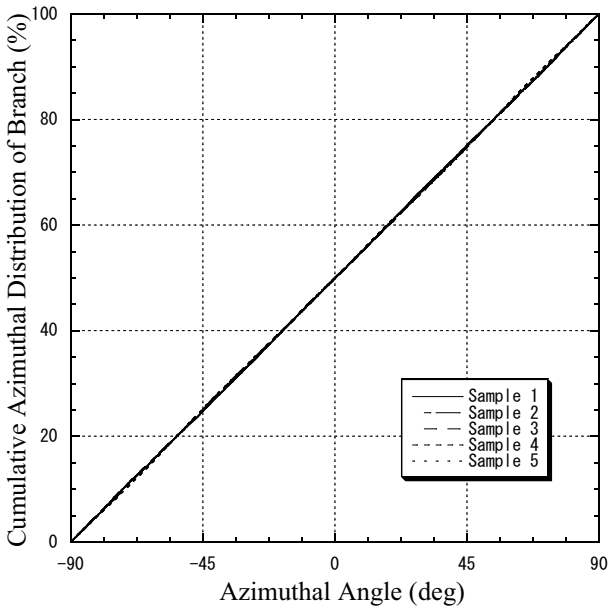

Figure 4. Cumulative azimuthal distributions of branch orientations.

line, while the distributions are uniform in the horizontal plane. In the present paper, we use both the cumulative azimuthal and zenithal distributions of branch orientations in more detail and better accuracy.

Before calculating both of the angular distributions, let us introduce the spherical polar coordinate (r, θ, φ), where θ and φ are the zenithal and azimuthal angles, respectively. The zenithal angle is measured from the z-(vertical) axis, while the azimuthal angle is from the x-axis in the $x - y$ plane. The zenithal and azimuthal angles of the k-th branch ($k = 1, 2, \ldots, N$, with N being the total number of branches) are denoted by θ_k and φ_k, respectively.

First, to examine the azimuthal distribution of branch orientations, consider the domain of

$$\varphi, \quad (-\pi/2, \pi/2].$$

If φ_k is in $(\pi/2, \pi]$, φ_k should be replaced by $\varphi_k - \pi$; similarly, that in $(-\pi, \pi/2]$ by $\varphi_k + \pi$. Furthermore, we rearrange the branches in ascending order of azimuthal angles in the range of $(-\pi/2, \pi/2]$. We define the cumulative frequency of the branch orientations in the following way:

$$F(\varphi) = \left(\frac{1}{\sum_{k=1}^{N} \sin\theta_k} \sum_{k=1}^{N} \sin\theta_k H(\varphi - \varphi_k) \right) \times 100(\%), \tag{3}$$

where $H(\varphi)$ is the Heaviside step function. $F(\varphi)$ with $\sin\theta_k$ as weight shows the cumulative percentage of the number of branches.

The cumulative azimuthal distribution defined above is calculated for all five samples. The results are shown in Figure 4. It can be seen that the cumulative distribution is almost exactly a straight line with gradient of 100/180. No sample seems to have any distinct characteristics. Thus, we conclude that the

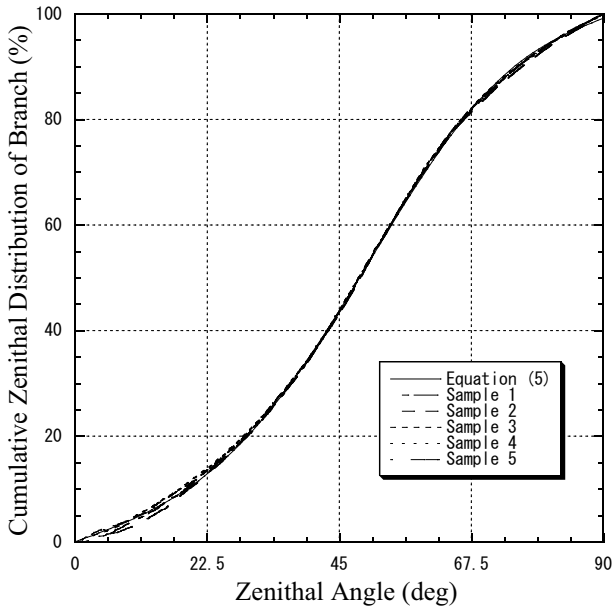

Figure 5. Cumulative zenithal distributions of branch orientations and their fitting curve given by Equation (5).

structure of the obtained random packings is isotropic in the horizontal $x - y$ plane in terms of the branch orientations.

Next, we examine the cumulative zenithal distribution of branch orientations. Similarly to the cumulative azimuthal distribution, θ_k should be replaced by $\theta_k - \pi/2$ if it is in $(\pi/2, \pi]$. We rearrange the branches in ascending order of azimuthal angles in the range of $(0, \pi/2]$. Since the circle made by $\theta = \theta_k$ on a sphere of unite radius is $2\pi \sin\theta_k$ in circumference, the cumulative frequency of branches per unit area of the sphere $F(\theta)$ is defined by

$$F(\theta) = \left(\frac{1}{\sum_{k=1}^{N} \frac{1}{\sin\theta_k}} \sum_{k=1}^{N} \frac{H(\theta - \theta_k)}{\sin\theta_k} \right) \times 100(\%). \tag{4}$$

The cumulative frequency is calculated and shown in Figure 5 for all samples. From this figure, it can be seen that the cumulative frequency distribution is not linear at all. Since the frequency distribution of branches is an odd function both about $\theta = 0°$ and $\theta = 90°$, we can express the distribution by the Fourier series of $\sin 2m\theta$. If we take into account only the first four terms, the distribution is

$$F(\theta) = a_0\theta + \sum_{m=1}^{3} \frac{a_m}{2m} \sin 2m\theta, \tag{5}$$

$$a_0 = 63.043, \qquad a_1 = -7.4308, \qquad a_2 = -38.522, \qquad a_3 = 7.5564,$$

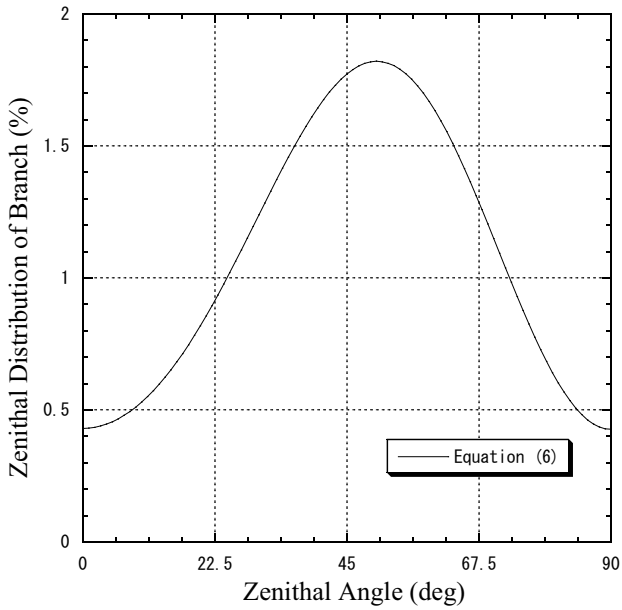

Figure 6. Zenithal distributions of branch orientations obtained from fitting curve, given by Equation (6).

where the four coefficients a_m have been determined by the least square method. The fitting curve of Equation (5) is drawn by a solid line in Figure 5; it cannot be distinguished from the original five curves, which reveals that the fitting is complete.

Differentiating Equation (5) with respect to θ, we obtain

$$\frac{dF(\theta)}{d\theta} = \sum_{m=0}^{3} a_m \cos 2m\theta. \tag{6}$$

This equation shows the zenithal distribution of branches itself and its curve is drawn in Figure 6. It is seen that the maximum frequency exists between 50° and 60° while the minimal is at $\theta = 0°$. By setting the derivative of Equation (6) to zero, $d^2F(\theta)/d\theta^2 = 0$, it is found that the frequency distribution has its peak at $\theta = 50.1°$. This peak position is correct because the present evaluation is more precise than that given by Kato et al. [2002]; their peak position $\theta = 45°$ was too rough.

From the arguments so far in this subsection, we can conclude that the packing structures are transversely isotropic, indicating the effect of gravity. This conclusion comes from the viewpoint of branch orientations.

4. Evaluation of spring constants of a sintered pair of balloons

4.1. ***Model of finite element.*** In the sintering of the balloon aggregate, necks are created around contact points of the balloons by mass diffusion; the necks grow up with sintering time. However, we do not simulate it, because we do not need to know its whole process, but need only to obtain the geometry of

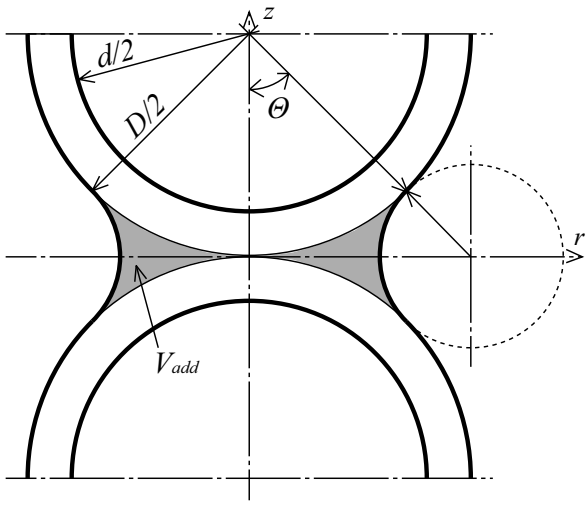

Figure 7. Geometry of a sintered (mass-added) balloon.

sintered state of aggregates. In order to represent the sintered geometry around the point of contact of paired balloons, we add around it some mass of the same substance as that of the balloons; the added volume is that bounded by the two contact balloons and a torus touching both of them, as shown in Figure 7. The geometry made by adding some mass is not exactly the same as that of real sintered balloon particles, but at least the shape of the void space in the mass-added spherical aggregate is much more similar to the real one than the infinitely long needle shape [Kurashige et al. 1992], which was assumed when the self-consistent models [Wu 1966; Berryman 1981] were applied. In Figure 7, D and d are the outer and inner diameters of the balloon, respectively. This added geometry was also used in [Sanders and Gibson 2003b; Sanders and Gibson 2003a].

The added volume per contact point can be calculated by simple geometrical consideration as

$$V_{\text{add}} = \frac{\pi}{4}\left(\frac{1-\cos\Theta}{\cos\Theta}\right)^2\left\{1-\left(\frac{\pi}{2}-\Theta\right)\tan\Theta\right\}\times D^3, \tag{7}$$

where Θ is the angle depicted in Figure 7. We will adopt the angle Θ as a parameter of sintering degree; we call it a *sintering degree angle*. In [Sanders and Gibson 2003b; Sanders and Gibson 2003a], this is called a *bond angle*.

4.2. ***Results of FEM analysis.*** The spring has six degrees of freedom: one for elongation and torsion, and two for bending and shearing. The spring constants are defined in the same manner as in the conventional structural analysis. Consider an hour glass shape of the two sintered half balloons shown in Figure 7. Fix its one end and give some generalized displacement on the other end; then we calculate the corresponding generalized forces, which provide the required spring constants. As a function of sintering degree angle Θ, we can obtain K_{ex} and M_{tx} for axial elongation $u_x = 1\times10^{-5}D$ and torsional angle $\theta_r = 1\times10^{-2}$, respectively; K_{bx} and M_{bz} for bending angle and K_{sy} and M_{sz} for lateral displacement. With respect to these notations, K and M correspond to the associated force and moment (or torque); the

first subscript represents the deformation modes, while the second one describes displacement direction or rotation axis. Notice that $K_{sz} = K_{sy}$, $M_{sy} = M_{sz}$ and $K_{bz} = K_{by}$ because of the geometrical axisymmetry.

We employ triangular ring elements. Numbers of nodes and elements are 2640 and 4949, respectively, for the thickest-walled balloons, while the thinnest-walled model contains 9989 nodes and 18545 elements. The numbers of nodes and elements are enough to evaluate the spring constants, as has been checked for the case of the smallest sintering angle by varying these numbers.

The FEM calculations have been carried out setting the Poisson's ratio of the balloon material to 0.25. It is reported in [Sanders and Gibson 2003b] that varying the Poisson's ratio has a negligible effect on the overall response.

All the spring constants normalized by Young's modulus of the balloon substance E_s versus the sintering degree angle Θ are given in Figures 8a to 8f for various inner/outer diameter ratios d/D ranging from 0.0 — 0.9 with their increment being 0.1. Figures 8a and 8b show K_{ex} for the axial elongation and M_{tx} for the torsion, respectively. Figures 8c and 8d depict K_{bx} and M_{bz} for the bending. Shown in Figures 8e and 8f are K_{sy} and M_{sz} for the lateral displacement with no gradient at the end, respectively. For all inner/outer ratios, these spring constants monotonically increase with the sintering angle, seeming to converge to zero with vanishing angle. Notice that $K_{bx} = M_{sz}$ because of the reciprocal relation. We confirmed that these spring constants numerically satisfy this relation (see Figures 8c and 8f).

These spring constants will be used to evaluate the macroscopic, effective or overall elastic moduli of the aggregate in the next section. Since the average coordination number for the random packing constructed is approximately 6.02, and very near to 6 for the regular simple cubic packings, we will simulate the tensile and shear tests up to the range of $\Theta = 45°$ in the next section. The lower limit is set to 3°.

5. Macroscopic material properties

5.1. ***Simulation method.*** Now, we will do tensile and shear tests of a *random network* of springs, with rigid hinges, of six degrees of freedom with the estimated spring constants. The random network is a mechanical model of sintered balloons. The model might be satisfactory if deformation of each hourglass-shaped spring is concentrated around its neck or near the sintered portion. This concentrated deformation for all springs would account for the overall deformation of the sintered aggregate. To confirm this is the case, we calculate strain energy density within the balloon pair from the above FEM analysis. The results are shown in Figure 9 for the case of a rather thin and well sintered balloon, $d/D = 0.9$ and $\Theta = 30°$. From this figure, it is seen that the high density region is near the sintered portion. Although the results are not illustrated here, the strain energy density obtained by the further FEM calculation depicts that the deformation occurs only around the neck even in the case of a thin neck, e.g., $\Theta = 5°$, independently of the balloon wall thickness. This argument reveals that both ends of the hourglass-shaped spring, which are far from the neck or sintered portion, is little deformed and plays a roll of the rigid hinge.

Since it was found that more spheres are in contact with others around the direction of $\theta = 50.1°$ from the vertical line, the porous media modeled by the random networks are expected to be transversely isotropic in their elastic moduli. So, we carry out both the three different tensile tests and shear tests of the networks. From the tensile tests, we obtain the macroscopic Young's moduli E_x^*, E_y^* and E_z^* and

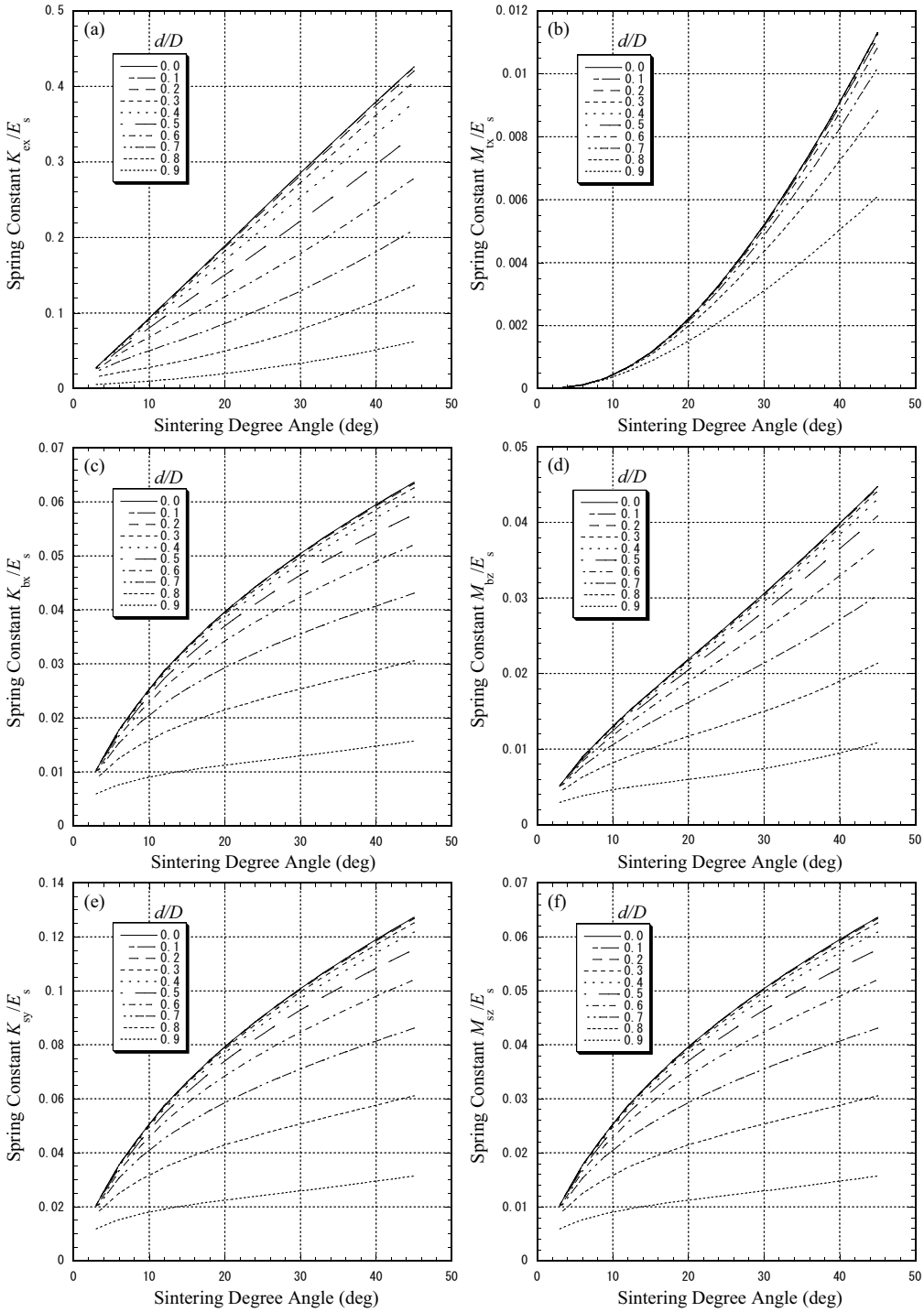

Figure 8. Spring constants versus sintering degree angle for (a) elongation; (b) torsion; (c) & (d) bending; and (e) & (f) shearing.

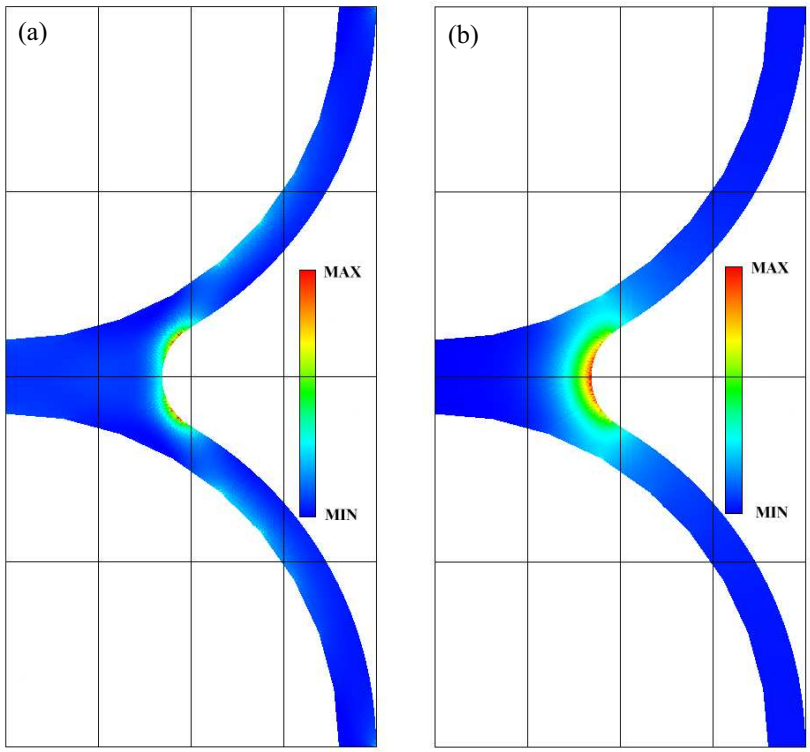

Figure 9. Distribution of strain energy density for (a) elongation and (b) torsion.

Poisson's ratios ν_{xy}, ν_{xz}, ν_{yx}, ν_{yz}, ν_{zx}, ν_{zy} according to their definition. Furthermore, we obtain G_{xy}, G_{xz} and G_{yz} from the shear tests.

We use a program for the 3D structural analysis, which is borrowed from a textbook [Beaufait et al. 1970], to simulate both of the tests.

5.2. ***Numerical results.*** Figures 10 and 11 respectively show macroscopic Young's moduli and shear moduli versus the total porosity in the sintered state; it should be noted that this porosity accounts for the hollow space of all the balloons as well, and that the added volume around all necks by sintering is subtracted from the whole void space. Although we have calculated all these moduli for all samples, we will present only graphs for sample 1, because we can see little difference among the samples for all diameter ratios. In all the figures, the ordinate presents their macroscopic Young's moduli E^* or shear moduli G^* normalized by Young's modulus of the balloon substance E_s; d/D is adopted as a geometrical parameter.

Figure 10 shows the porosity dependence of Young's moduli E_x^*/E_s, while Figure 11 shows G_{xy}^*/E_s.

Comparing the results in Figure 10 with those in the figure for E_z^* omitted for brevity, we find that the value of E_z^* is roughly 20% larger than E_x^* over the entire region of porosity for all diameter ratios. This can be understood from the following facts: all springs lying in the direction of around 50.1° from the

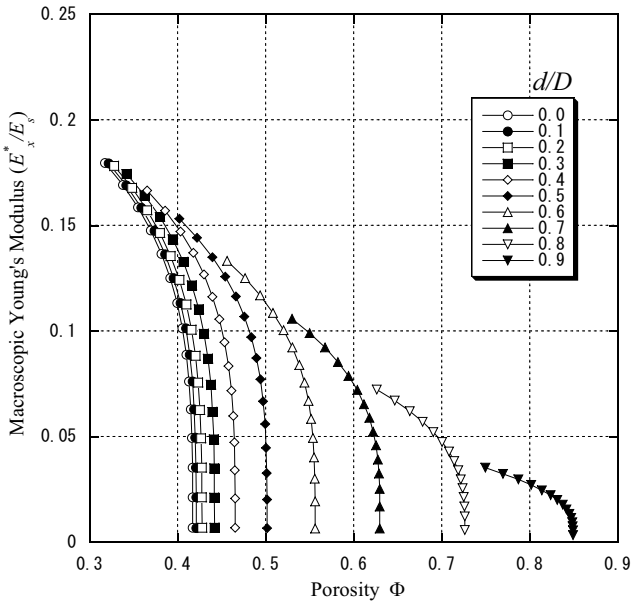

Figure 10. Young's moduli in isotropy plane versus porosity.

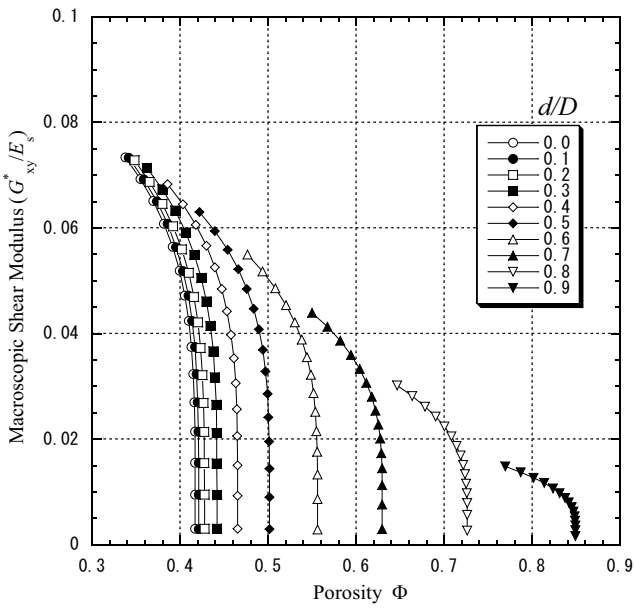

Figure 11. Shear moduli in isotropy plane versus porosity.

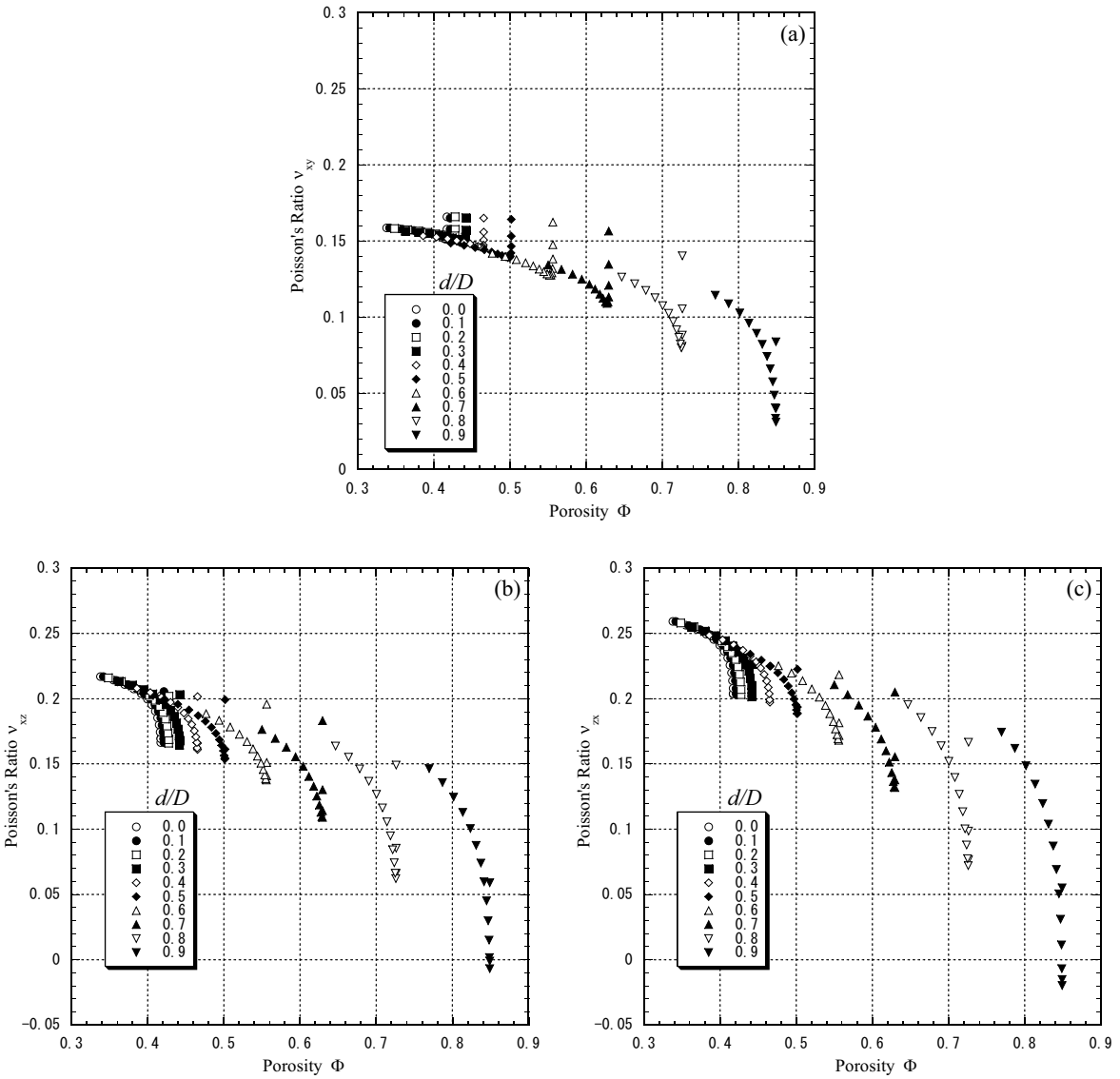

Figure 12. Three independent Poisson's ratios versus porosity: (a) ν_{xy}, (b) ν_{xz} and (c) ν_{zx}, for d/D ranging from 0.0—0.9

vertical line support forces in the z direction, while only some parts of them lying around the $x-z$ plane support forces in the x direction but some parts of them lying around the $y-z$ plane do not. Similarly, G^*_{xy} shown in Figure 11 is larger than G^*_{xz}, not shown, by more than approximately 30% over the whole range of porosity. Furthermore, we can numerically confirm, although not shown, that $E^*_x = E^*_y$ and $G^*_{xz} = G^*_{yz}$. These observations show again that the packing structure of the simulation is of transverse isotropy.

Next, we examine dependence of the elastic moduli on the degree of sintering and the diameter ratio; each marker on an individual curve in both the figures corresponds to the sintering degree angle ranging from 3° to 45° at the interval of 3°; and progress toward the right on the curve makes the sintering degree low. For each constant diameter ratio, the smaller the degree of sintering is, the smaller the elastic moduli. Increases in the diameter ratio lower the curves as a whole, especially so for the higher degree of sintering. They also shift the curves toward higher porosity as a whole, because the balloon wall becomes thinner. The elastic moduli are little affected by the ratio if the ratio is smaller or for the thicker balloon wall. The elastic moduli lowers rapidly if the diameter ratio is larger than 0.5. The elastic modulus of the aggregate of hollow spheres with $d/D = 0.9$ is approximately a quarter of that of solid spheres. All these things are valid for all the figures, including the omitted. This is also true for Young's moduli E_y^* and for shear moduli G_{yz}^*, as confirmed by further calculation.

It should be added that both Young's and shear moduli go to zero as the sintering angle tends to zero for all the diameter ratios even for a finite value of the porosity; the porosity depends on the diameter ratio as well as on the sintering angle and packing structures.

In the above, we have mentioned that Young's modulus E_z^* and shear modulus G_{xz}^* are larger than E_x^* and G_{xy}^* by 20% and 30%, respectively. These moduli, however, depend on the diameter ratio and sintering angle in a very complicated manner, so the degree of anisotropy cannot be described by a simple multiplication factor. Therefore, it may be important for practical purposes to express all the elastic moduli in terms of a simple—that is, polynomial—expression of the two geometrical parameters d/D and Θ. The expressions are determined by the conventional least square method as follows:

$$\frac{E_x^*}{E_s} = \left(4.24\times10^{-3} + 2.91\times10^{-3}\frac{d}{D} - 7.45\times10^{-3}\left(\frac{d}{D}\right)^2\right)\Theta + \left(-5.42\times10^{-6} - 2.57\times10^{-5}\frac{d}{D} + 3.43\times10^{-5}\left(\frac{d}{D}\right)^2\right)\Theta^2, \quad (8)$$

$$\frac{E_z^*}{E_s} = \left(5.28\times10^{-3} + 6.64\times10^{-3}\frac{d}{D} - 9.27\times10^{-3}\left(\frac{d}{D}\right)^2\right)\Theta + \left(-1.16\times10^{-5} - 3.42\times10^{-5}\frac{d}{D} + 4.96\times10^{-5}\left(\frac{d}{D}\right)^2\right)\Theta^2, \quad (9)$$

$$\frac{G_{xy}^*}{E_s} = \left(1.82\times10^{-3} + 1.27\times10^{-3}\frac{d}{D} - 3.16\times10^{-3}\left(\frac{d}{D}\right)^2\right)\Theta + \left(-4.17\times10^{-6} - 1.15\times10^{-5}\frac{d}{D} + 1.6\times10^{-5}\left(\frac{d}{D}\right)^2\right)\Theta^2, \quad (10)$$

$$\frac{G_{xz}^*}{E_s} = \left(2.25\times10^{-3} + 1.44\times10^{-3}\frac{d}{D} - 3.9\times10^{-3}\left(\frac{d}{D}\right)^2\right)\Theta + \left(-2.07\times10^{-6} - 1.33\times10^{-5}\frac{d}{D} + 1.75\times10^{-5}\left(\frac{d}{D}\right)^2\right)\Theta^2. \quad (11)$$

All the equations are valid for $0.0 \leq d/D \leq 0.9$ and $3^\circ \leq \Theta \leq 45^\circ$ to within 8.5%.

Now, we will move on to discuss Poisson's ratio. The topic is a little more complicated than that of the Young's and shear moduli.

Figures 12a — c show the behavior of Poisson's ratios, ν_{xy}, ν_{xz}, ν_{zx}, respectively, against the total porosity for various inner/outer diameter ratios d/D ranging from 0.0 — 0.9 with their increment being 0.1; ν_{xy} means Poisson's ratio in the isotropy plane; ν_{xz} denotes the contraction ratio in the z axis under uniaxial tension in the x direction, while ν_{zx} the one in the x axis under z tension. The estimation of all Poisson's ratios here are based on the described definitions; in other words, not on some relations among other elastic moduli estimated.

The macroscopic Poisson's ratio obtained is smaller than that of the balloon substance $\nu = 0.25$ with exceptional cases of ν_{zx}, for very small porosity and small diameter ratios. It seems to be a general tendency that Poisson's ratio of porous materials is smaller than that of the original material. Few papers report on this topic but Sanders and Gibson [2003a] give much smaller Poisson's ratios for the BCC and FCC packings than the original one.

In Figure 12, it can be seen that the dependence of Poisson's ratios on porosity is similar to that of Young's and shear moduli. The ratios decrease with decreasing sintering degree angle for each diameter ratio. They are little affected by the diameter ratio if it is smaller (or for the thicker balloon wall), more precisely for $d/D < 0.4$. The Poisson's ratios decrease rapidly if the diameter ratio is larger than 0.5. Poisson's ratio ν_{xy} in the isotropy plane is the smallest, while ν_{zx} is the largest; ν_{xz} lies between them.

It is interesting that all Poisson's ratios sharply ascend with an approach of porosity to the nonsintered state. This is supported by the similar ascent for the solid sphere aggregates obtained by Kato et al. [2002], but it may be true on condition that these results are sufficient in their accuracy in the limit.

We have already given the formulae to estimate the four elastic moduli. The final modulus of five independent moduli for transversely isotropic media, if we select ν_{zx}, can be expressed in terms of d/D and Θ as follows:

$$\nu_{zx} = \left(1.38 \times 10^{-1} + 3.19 \times 10^{-3}\left(\frac{d}{D}\right)^{2.2} - 5.41 \times 10^{-1}\left(\frac{d}{D}\right)^{5.2}\right)\Theta^{0.1} + \left(8.1 \times 10^{-3} - 2.16 \times 10^{-3}\left(\frac{d}{D}\right)^{1.2} + 1.18 \times 10^{-1}\left(\frac{d}{D}\right)^{6.8}\right)\Theta^{0.5}. \quad (12)$$

The equation describes the results for $0.0 \leq d/D \leq 0.9$ and $9^\circ \leq \Theta \leq 45^\circ$ to within 10% in all cases. Note that the lower limit of the sintering degree is 9° to avoid the rapid ascent in the ratio in approaching the nonsintered state; the relative error is larger for the degree smaller than that. More important, the expression given by Equation (12) is not a polynomial of d/D and Θ, because the dependence of the ratio on these parameters is too complicated to express by means of a polynomial.

For the transverse isotropy in elasticity, the reciprocal relations

$$\frac{\nu_{xz}}{E_x^*} = \frac{\nu_{zx}}{E_z^*}, \qquad \frac{\nu_{yz}}{E_y^*} = \frac{\nu_{zy}}{E_z^*} \quad (13)$$

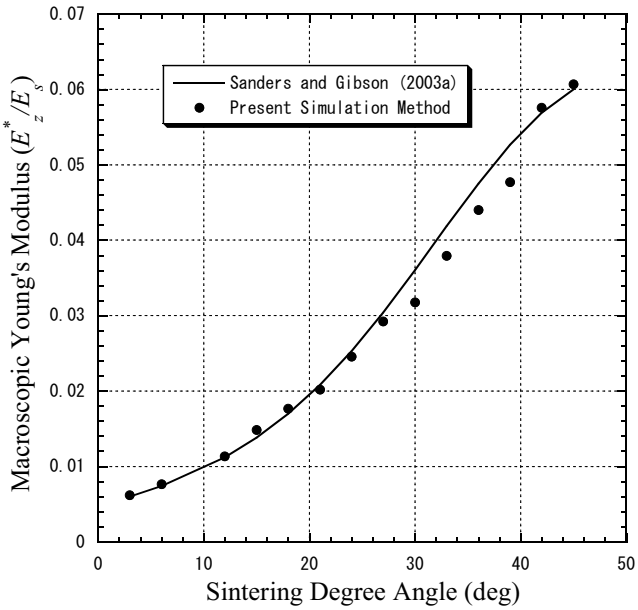

Figure 13. Relative Young's modulus in [100] for SC packing calculated by present method versus sintering degree angle together with that of [Sanders and Gibson 2003b].

must be fulfilled. Poisson's ratio ν_{xz} can be determined from the first relation. In addition, $\nu_{yz} = \nu_{xz}$ and $\nu_{zy} = \nu_{zx}$. We have confirmed that the present results almost satisfy these relations.

Poisson's ratio ν_{xy} can be expressed in terms of E^*_x and G^*_{xy} as

$$\nu_{xy} = \frac{E^*_x}{2G^*_{xy}} - 1. \tag{14}$$

However, Poisson's ratios ν_{xy} calculated by Equation (14) differ considerably from the simulated ones. If G^*_{xy} deviates by $\pm 5\%$ in Equation (14), the ν_{xy} varies by as much as 30%. Thus, we cannot use Equation (14) to determine Poisson's ratio ν_{xy}. Instead, it can be obtained from the following expression in terms of d/D and Θ in a manner similar to that of Equation (12):

$$\nu_{xy} = \left(7.96 \times 10^{-2} - 2.24 \times 10^{-1}\left(\frac{d}{D}\right)^{1.9} + 3.48 \times 10^{-1}\left(\frac{d}{D}\right)^{2.5}\right)\Theta^{0.4} + \left(-1.01 \times 10^{-2} - 5.2 \times 10^{-2}\left(\frac{d}{D}\right)^{1.9} + 7.68 \times 10^{-2}\left(\frac{d}{D}\right)^{2.5}\right)\Theta^{0.8}. \tag{15}$$

The equation describes the results for $0.0 \le d/D \le 0.9$ and $9^\circ \le \Theta \le 45^\circ$ to within 10% in all cases.

We have determined the in-plane shear modulus G^*_{xy} from the shear tests. However, we can calculate G^*_{xy} from only the tensile test using Equation (14). So we estimate G^*_{xy} from Equation (14). The results fit those from the shear test to within $\pm 5\%$.

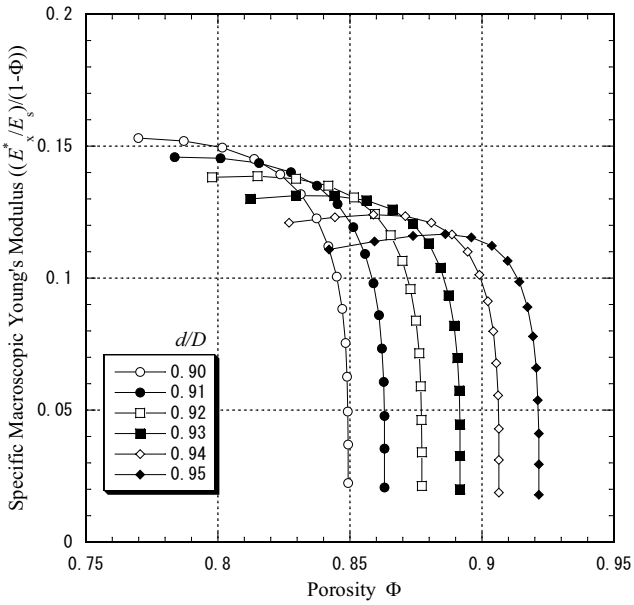

Figure 14. Specific Young's moduli in isotropy plane versus porosity for d/D ranging from 0.9 — 0.95.

6. Discussion

6.1. ***Validity of the proposed simulation method.*** We have simulated the elastic properties of randomly packed sintered balloons using the three-step simulation method. Here, we will confirm validity of the present method by applying it to the simple cubic packing.

[Sanders and Gibson 2003b] evaluated the mechanical properties of simple cubic packed hollow-sphere foams by the FEM analysis of a unit cell with the periodic boundary conditions. We calculate the relative Young's and shear moduli for the same SC packings by the present method. Figure 13 compares the relative Young's modulus for the SC packing calculated by the present method with that obtained from the formula given by [Sanders and Gibson 2003b]. A good agreement is seen between them for a wider range of the sintering degree angle, although Sanders and Gibson pointed out that their formula is applicable to the range from 10° to 40°.

6.2. ***Better design; larger specific moduli.*** One of the advantageous properties of the sintered balloon compacts is a high specific modulus. To consider the better design of compacts, we examine a specific relative modulus, which is defined as the relative effective modulus divided by the relative effective density of a sintered aggregate, where the term *relative* means the quantity divided by that of the original balloon material. In what follows, this term will be omitted in almost all cases. We have calculated the specific Young's and shear moduli for a wide range of the diameter ratios, but will not show all of them. In Figures 14 and 15, we will show the specific moduli only for the case of the diameter ratio larger than 0.9, because commercially available balloons have rather thin walls. Both figures illustrate the moduli in the isotropy plane.

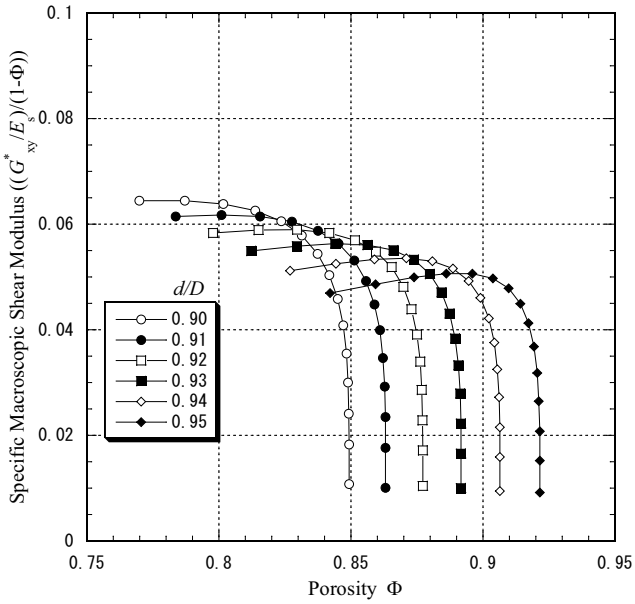

Figure 15. Specific shear moduli in isotropy plane versus porosity for d/D ranging from 0.9 — 0.95.

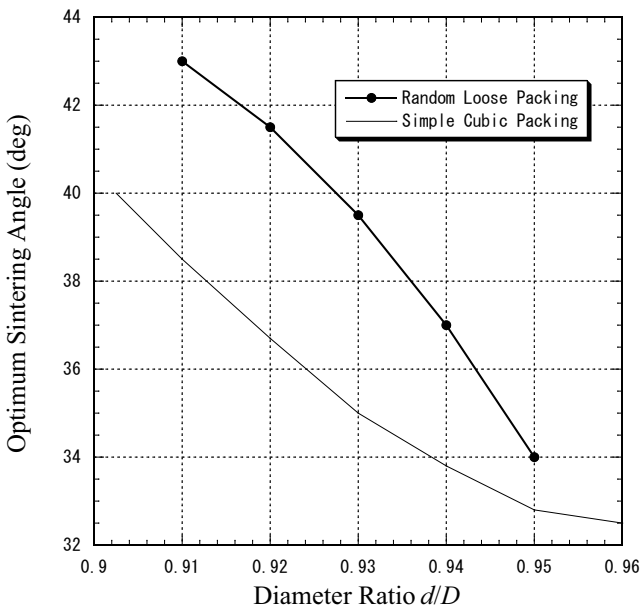

Figure 16. Optimum sintering degree angle plotted as a function of inner/outer diameter ratio for random and SC packings.

In the first place, we have to point out that the curves of the specific moduli against the porosity have a peak both for Young's and shear moduli in the isotropy plane. This is also true for those out of the plane.

It seems that there is a complicated mechanism behind the peak occurrence. Let us consider the case of Young's modulus, so that it may be enough to refer to only Figure 14 and, in addition, Figure 10 for comparison. See the curve of $d/D = 0.9$ in the latter figure; it can be seen that the modulus gradually slows down with increase in porosity for the smaller porosity range and rapidly falls down for the larger porosity, approaching the point contact state; the gradual slow-down is caused by deformation of upper and lower thin shell parts around a neck and this deformation is not strongly affected by the sintering degree, while the sharp falling is due to the concentrated deformation near a contact point because of the less sintered state. On the other hand, because the balloon thickness is constant on the given curve, decrease in the porosity implies increase in the sintering degree. This increase makes the specific density rise; dividing the modulus depicted in Figure 10 by this increased specific density leads to the smaller specific modulus shown in Figure 14.

In many cases, the largest specific modulus is the optimum porous material with respect to rigidity. Figure 16 shows the optimum sintering angle for the Young's modulus, in the z direction, of sintered random packings, plotted as a function of the diameter ratio together with that given for the SC regular packings by [Sanders and Gibson 2003b]. It is seen that the optimum angle of the random packings higher than that of SC. It should be added that the Young's and shear modulus (the latter is not shown) in the isotropy plane have almost the same optimum sintering angle and the same thing is true for the moduli out of the plane (not shown).

In the material design, therefore, we must select the best sintering condition from this result.

6.3. ***Negative Poisson's ratios.*** Here, we will back to Figures 12a — 12c. Scrutinizing the figures, we find that the Poisson's ratios are negative in the case of very thin balloon wall and very low sintering degree. Because of this interesting characteristic, we have calculated the Poisson's ratios for the case of $d/D = 0.8$ or more in detail and shown them in Figures 17a — 17c.

The negative Poisson's ratio implies that the uniaxial tensile (compressive) load applied on a body will lead to its expansion (contraction) in the direction orthogonal to the applied load.

A foam with negative Poisson's ratio was first fabricated by Lakes [1987]. In general, typical microstructures of foams with negative Poisson's ratio are of three types: inverted *re-entrant* cell shape [Lakes 1987; Friis et al. 1988], solid particles attached to each other by elastic strips [Lakes 1991; Prall and Lakes 1997] and nodes, connected by tensile springs, constrained by hinged inextensible rods [Evans and Caddock 1989]. However, the slightly sintered random balloon aggregates have none of such structures as mentioned just in the above.

Using the discrete element method for a random granular material, Bathurst and Rothenburg [1988] and Alzebdeh and Ostoja-Starzewski [1999] showed that effective Poisson's ratio for an aggregate of two-dimensional irregular particles is negative in some cases even when the individual Poisson's ratios of particles are positive. Bathurst and Rothenburg [1988] examined negative Poisson's ratio behavior by varying the ratio of a normal stiffness and shear stiffness between particles. They found that the Poisson's ratio is negative when the shear stiffness is higher than the normal stiffness.

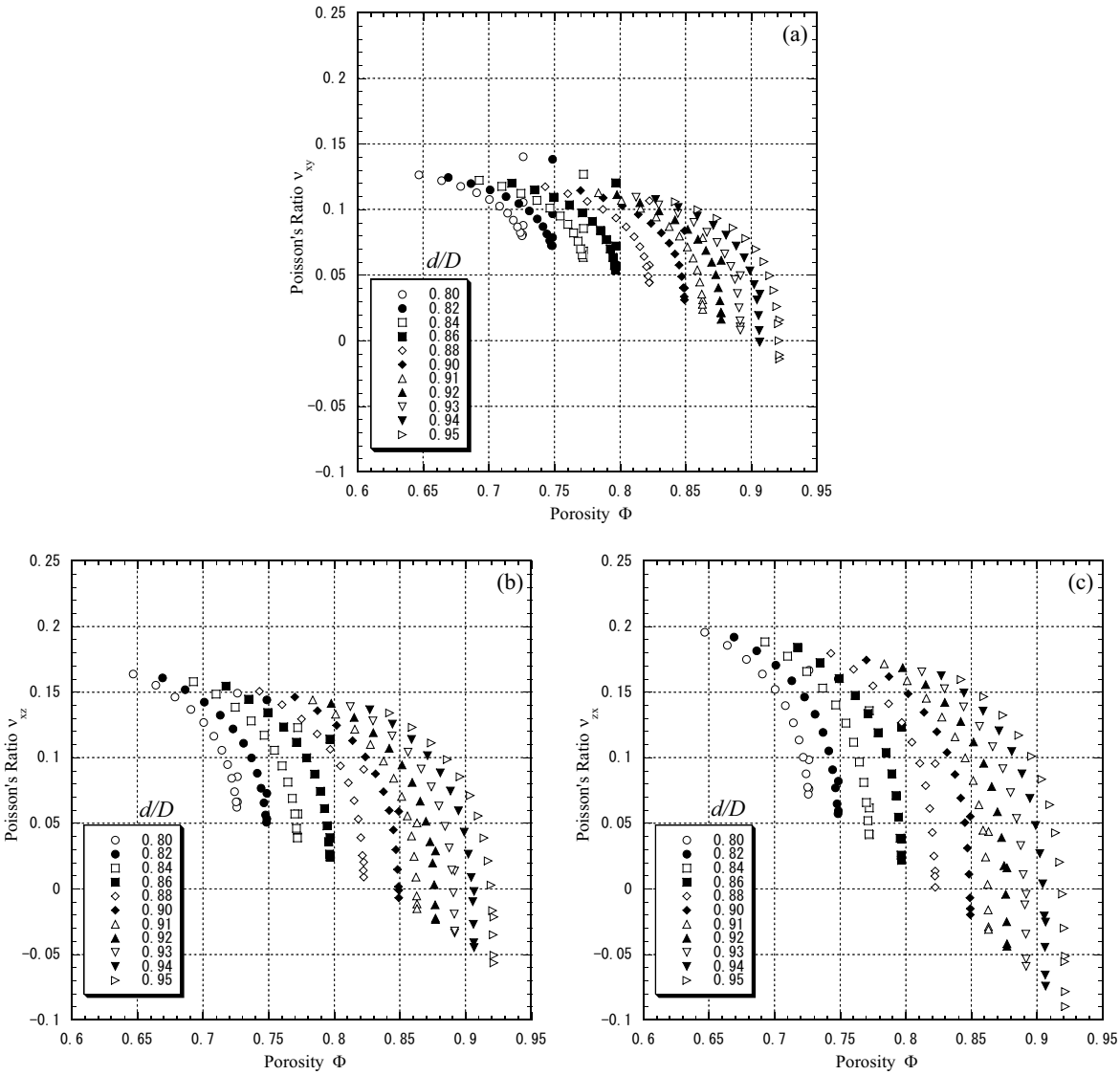

Figure 17. Three independent Poisson's ratios versus porosity: (a) ν_{xy}, (b) ν_{xz} and (c) ν_{zx}, for d/D ranging from 0.8 — 0.95.

Following their discussion, we pick up only the shear stiffness K_{sy} and normal stiffness K_{ex} of a connected balloon pair from the six spring constants calculated in the above FEM analysis. For a solid sphere of $d/D = 0.0$, if the sintering degree angle varies down from 45° to 3° (this descending degree means the shift of the markers toward the right or higher porosity on each curve in Figure 12), their ratio K_{sy}/K_{ex} changes from 0.2 to 0.37, whereas, for a thinner balloon of $d/D = 0.9$, the ratio changes from 0.5 to 2.1. A rough estimate of the variation of the Poisson's ratio against that of the stiffness ratio shows that the Poisson's ratios are negative when K_{sy}/K_{ex} is greater than 2. More precisely, this critical value

slightly differs from each other for the three independent Poisson's ratios; remember that we have the three distinct ratios because the sintered aggregates under consideration are transversely isotropic.

6.4. ***Comparison with SC packing.*** Finally, we compare the Young's modulus of the present random loose (RL) packing with that of the regular packing. Here, we select the SC packing from among regular packings, because the average coordination number for the random packing constructed is approximately 6 and very near to that for the regular SC packings, whose coordination number is exactly 6. It should be mentioned here that the present RL packing is of axial symmetry with the five independent elastic moduli while the SC packing is of cubic symmetry with the three.

In Figure 18, the Young's moduli, E_x^* and E_z^*, of the RL packing are plotted versus the sintering degree in the case of $d/D = 0.9$. Also shown in the figure are the Young's moduli in the [1 0 0], [1 1 0] and [1 1 1] directions for the SC packing for the same d/D; these moduli are calculated by using the standard transformations of elastic moduli from the three compliances, S_{11}, S_{12} and S_{44}, in the form of the fitting formula given by [Sanders and Gibson 2003b].

A good agreement is seen between the Young's modulus of the random packing in the z direction and that of the SC in the [1 0 0] direction only when $\Theta < 20°$. However, for $\Theta > 20°$, the latter is greater than the former; the difference between them increases with increasing sintering degree angle. For the sintering degree angle $\Theta = 30°$ and diameter ratio $d/D = 0.9$, the relative Young's modulus is 38% greater in the [1 0 0] direction of SC than in the z direction for the RL packing. For the same sintering degree angle and diameter ratio, the relative Young's modulus in the [1 1 0] and [1 1 1] directions of SC are 1.86 and 2.11 times that in the z direction for the RL packing.

Figure 19 shows the Young's modulus versus porosity for both the RL and SC packings when we have $d/D = 0.9$ and 0.95. For each diameter ratio, the Young's modulus of RL packing is much smaller than that of the regular SC stacking, although the difference between them is rather small when the sintering degree angle is about 20°. It can be concluded that, although the average coordination number for the random packing constructed is very near to that for the regular SC packings, the macroscopic properties of the RL packing are significantly different from those of the packing in elasticity and anisotropy.

7. Conclusions

We have evaluated the macroscopic elastic properties of the sintered, randomly packed balloons for various degrees of sintering and for a wide range of the balloon wall thickness. The conclusions are summarized below:

(1) The packing structure in the vertical direction is different from that in other directions. Branches lie more frequently around the direction of 50.1° from the vertical line than other directions, whereas they are uniformly distributed about the vertical line. The packings constructed by the present method are of transverse isotropy; in other words, the structure is affected by gravity.

(2) The elastic moduli are little affected by the diameter ratio for thicker balloons whose ratio is less than about 0.4, while the properties of thinner balloons are very sensitive to the ratio; they rapidly decline with decreasing wall thickness of the balloons.

(3) The moduli are larger in the direction of gravity than in the horizontal one, as expected for the gravity-affected packing structures.

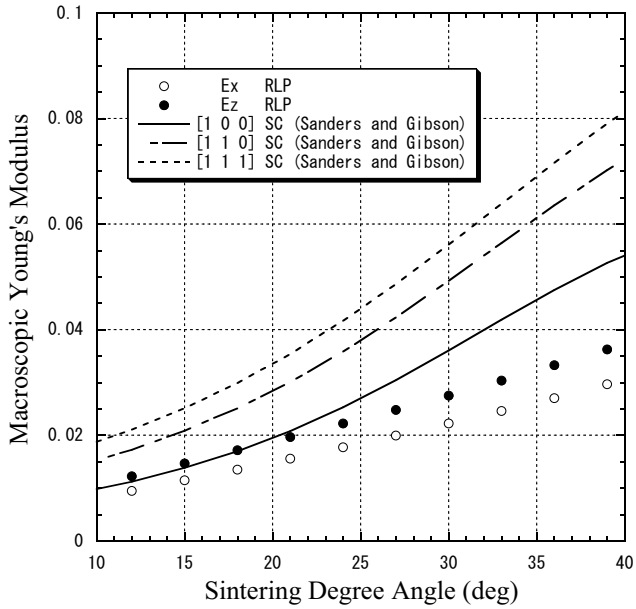

Figure 18. Relative Young's modulus plotted against sintering degree angle for random loose packing and SC packing.

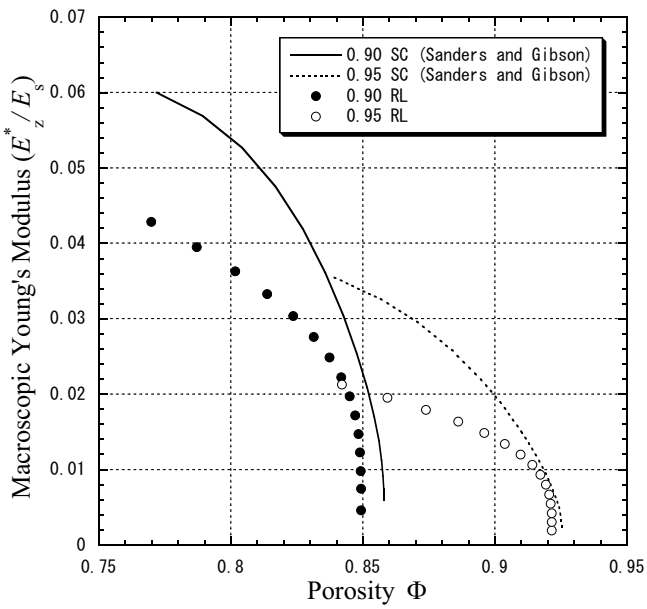

Figure 19. Relative Young's modulus plotted against porosity for random loose packing and SC packing for $d/D = 0.9$ and 0.95.

(4) The specific elastic moduli are found to have a peak when the balloons have a diameter ratio larger than about 0.9.

(5) The Poisson's ratios are slightly negative in the case of very thin balloon walls and very low sintering degree.

(6) The macroscopic properties of the RL packing are significantly different from those of the SC packing in elasticity and anisotropy, although the both packings have almost the same coordination number.

References

[Alzebdeh and Ostoja-Starzewski 1999] K. Alzebdeh and M. Ostoja-Starzewski, "On a spring-network model and effective elastic moduli of granular materials", *J. Appl. Mech.* (*ASME*) **66** (1999), 172–180.

[Andersen et al. 2000] O. Andersen, U. Wang, L. Schnerder, G. Stephani, and B. Kieback, "Novel metallic hollow sphere structures", *Adv. Eng. Mater.* **2**:4 (2000), 192–195.

[Andrews et al. 1999] E. Andrews, W. S. Sanders, and L. J. Gibson, "Compressive and tensile behaviour of aluminum foams", *Mater. Sci. Eng. A* **270**:2 (1999), 113–124.

[Ashby et al. 2000] M. F. Ashby, N. Evans, A. Fleck, L. J. Gibson, J. W. Hutchinson, and H. N. G. Wadley, *Metal foams: A design guide*, Butterworth-Heinemann, 2000.

[Bardella and Genna 2001] L. Bardella and F. Genna, "On the elastic behavior of syntactic foams", *Int. J. Solids Struct.* **38**:40 (2001), 7235–7260.

[Bathurst and Rothenburg 1988] R. J. Bathurst and L. Rothenburg, "Note on a random isotropic granular material with negative Poisson's ratio", *Int. J. Eng. Sci.* **26**:4 (1988), 373–383.

[Beaufait et al. 1970] F. W. Beaufait, W. H. Rowan, Jr, P. G. Hoadley, and R. M. Hackett, *Computer methods of structural analysis*, Prentice-Hall, Englewood Cliffs, NJ, 1970.

[Bennett 1972] C. H. Bennett, "Serially deposited amorphous aggregates of hard spheres", *J. Appl. Phys.* **43**:6 (1972), 2727–2734.

[Berryman 1981] J. G. Berryman, "Elastic wave propagation in fluid-saturated porous media", *J. Acoust. Soc. Am.* **69**:2 (1981), 416–424.

[Debbas and Rumpf 1966] D. Debbas and H. Rumpf, "On the randomness of beds packed with spheres or irregular shaped particles", *Chem. Eng. Sci.* **21**:6–7 (1966), 583–608.

[Evans and Caddock 1989] K. E. Evans and B. D. Caddock, "Microporous materials with negative Poisson's ratios, II: Mechanisms and interpretation", *J. Phys. D Appl. Phys.* **22**:14 (1989), 1883–1887.

[Friis et al. 1988] R. S. Friis, R. S. Lakes, and J. B. Park, "Negative Poisson's ratio polymeric and metallic foams", *J. Mater. Sci.* **23**:12 (1988), 4406–4414.

[Gasser et al. 2003] S. Gasser, F. Paun, A. Cayzeele, and Y. Bréchet, "Uniaxial tensile elastic properties of a regular stacking of brazed hollow spheres", *Scr. Mater.* **48**:12 (2003), 1617–1623.

[Gasser et al. 2004a] S. Gasser, Y. Brechet, and F. Paun, "Materials design for acoustic liners: an example of tailored multifunctional materials", *Adv. Eng. Mater.* **6**:1–2 (2004), 97–102.

[Gasser et al. 2004b] S. Gasser, F. Paun, and Y. Bréchet, "Finite element computation for the elastic properties of a regular stacking of hollow sphere", *Mater. Sci. Eng. A* **379**:1–2 (2004), 240–244.

[Gibson and Ashby 1997] L. J. Gibson and M. F. Ashby, *Cellular solids: structure and properties*, 2nd ed., Cambridge University Press, Cambridge, 1997.

[Haughey and Beveridge 1969] D. P. Haughey and G. S. G. Beveridge, "Structural properties of packed beds", *Can. J. Chem. Eng.* **47** (1969), 130–140.

[Kato et al. 2002] H. Kato, C. Matsunaga, M. Kurashige, and K. Imai, "Anisotropy in packing structure and elasticity of sintering spherical particles", *JSME Int. J. A Mech. M.* **45**:4 (2002), 585–595.

[Kurashige et al. 1992] M. Kurashige, K. Imaida, and Y. Goto, "Phase velocity measurement for three bulk waves in water-saturated sintered glass beads by an ultrasonic mode conversion method", pp. 508–513 in *Proceedings of the International Symposium on Impact Engineering* (Sendai), vol. 2, edited by I. Maekawa, 1992.

[Kurashige et al. 1999a] M. Kurashige, T. Hayashi, and K. Imai, "Simulated effective elastic moduli and wave velocities in water-saturated sintered glass-beads", *Acta Mech.* **132**:1–4 (1999), 177–194.

[Kurashige et al. 1999b] M. Kurashige, M. Mishima, and K. Imai, "Simulated effective thermal conductivity of sintered, randomly packed spheres and statistical structures of packings", *J. Therm. Stresses* **22**:7 (1999), 713–733.

[Lakes 1987] R. S. Lakes, "Foam structures with negative Poisson's ratio", *Science* **235**:4792 (1987), 1038–1040.

[Lakes 1991] R. S. Lakes, "Deformation mechanisms in negative Poisson's ratio: structural aspects", *J. Mater. Sci.* **26**:9 (1991), 2286–2292.

[Marur 2005] P. R. Marur, "Effective elastic moduli of syntactic foams", *Mater. Lett.* **59**:14–15 (2005), 1954–1957.

[Nolan and Kavanagh 1992] G. T. Nolan and P. E. Kavanagh, "Computer simulation of random packing of hard spheres", *Powder Technol.* **72**:2 (1992), 149–155.

[Norris and Gojny 1990] B. Norris and F. J. Gojny, "Hollow metal sphere filled stabilized skin structures and method of making", United States Patent. No. 4925740, 1990.

[Prall and Lakes 1997] D. Prall and R. S. Lakes, "Properties of a chiral honeycomb with a Poisson's ratio of -1", *Int. J. Mech. Sci.* **39**:3 (1997), 305–314.

[Queheillalt et al. 2002] D. T. Queheillalt, D. J. Sypeck, and H. N. G. Wadley, "Ultrasonic characterization of cellular metal structures", *Mater. Sci. Eng. A* **323**:1–2 (2002), 138–147.

[Sanders and Gibson 2003a] W. S. Sanders and L. J. Gibson, "Mechanics of BCC and FCC hollow-sphere foams", *Mater. Sci. Eng. A* **352**:1–2 (2003), 150–161.

[Sanders and Gibson 2003b] W. S. Sanders and L. J. Gibson, "Mechanics of hollow sphere foams", *Mater. Sci. Eng. A* **347**:1–2 (2003), 70–85.

[Taguchi et al. 2006] I. Taguchi, M. Kurashige, and K. Imai, "Effects of cubic container's wall or floor on random packing structures of spherical particles", *JSME Int. J. A Mech. M.* **49**:2 (2006), 265–272.

[Torobin 1986] L. B. Torobin, "Metal microspheres, filamented hollow metal microspheres and articles produced therefrom", United States Patent. No. 4582534, 1986.

[Torquato 2001] S. Torquato, *Random heterogeneous materials: microstructure and macroscopic properties*, Springer, New York, 2001.

[Tory et al. 1973] E. M. Tory, B. H. Church, M. K. Tam, and M. Ratner, "Simulated random packing of equal sphere", *Can. J. Chem. Eng.* **51** (1973), 484–493.

[Wadley 2002] H. N. G. Wadley, "Cellular metals manufacturing", *Adv. Eng. Mater.* **4**:10 (2002), 726–733.

[Wichmann and Hill 1982] B. A. Wichmann and I. D. Hill, "Algorithm AS 183: An efficient and portable pseudo-random number generator", *Appl. Stat.* **31**:2 (1982), 188–190.

[Wu 1966] T. T. Wu, "The effect of inclusion shape on the elastic moduli of a two-phase material", *Int. J. Solids Struct.* **2**:1 (1966), 1–8.

Received 23 Apr 2006. Accepted 31 Aug 2006.

ISAO TAGUCHI: isao_taguchi@pref.aomori.lg.jp
Graduate School of Engineering, Iwate University, Ueda 4-3-5, Morioka, Iwate 020-8551, Japan

MICHIO KURASHIGE: kurashige@iwate-u.ac.jp
Department of Mechanical Engineering, Iwate University, Ueda 4-3-5, Morioka, Iwate 020-8551, Japan